Applied Surface Science 282 (2013) 724–728

Contents lists available at SciVerse ScienceDirect

Applied Surface Science

journal homepage: www.elsevier.com/locate/apsusc

Positron annihilation Doppler broadening study of Xe-implanted aluminum

R.S. Yu [a,*], M. Maekawa [b], A. Kawasuso [b], B.Y. Wang [a], L. Wei [a]

[a] Key Laboratory of Nuclear Analysis Techniques, Institute of High Energy Physics, Chinese Academy of Sciences, No. 19 Yuquan Lu, Beijing 100049, China
[b] Japan Atomic Energy Agency, Advanced Science Research Center, Watanuki 1233, Takasaki, Gunma 370-1292, Japan

ARTICLE INFO

Article history:
Received 22 April 2013
Received in revised form 2 June 2013
Accepted 6 June 2013
Available online 25 June 2013

Keywords:
Positron annihilation
Doppler broadening
Vacancy
Xenon

ABSTRACT

Positron annihilation Doppler broadening measurements were conducted to characterize information of defects in 380 keV Xe^+-implanted aluminum upon thermal annealing at temperatures ranging from 100 to 600 °C. The results suggest a broad distribution in the depth of vacancy-type defects in all the as-implanted samples. Meanwhile, with an increase in implantation dose the defect-rich region shifts toward the sample surface. It was found that increasing the annealing temperature triggers surface-directed migration and coalescence of vacancy and Xe_nV_m clusters in samples with implantation doses of 1E15 and 1E16 $Xe^+ cm^{-2}$. In the sample implanted with a high dose of 1E17 $Xe^+ cm^{-2}$, positron annihilation revealed a decomposition and even elimination of such defects under post-implantation annealing treatment.

© 2013 Elsevier B.V. All rights reserved.

1. Introduction

Implantation of inert gas ions into solid materials has been studied extensively from the point of view of the application to nuclear energy. It is known that when Xe ions are implanted into aluminum, a fine dispersion of solid state Xe precipitates (often called bubbles) forms [1,2]. A great deal of work has been carried out to understand the nucleation, formation, growth, and segregation of these Xe bubbles [3,4]; however, knowledge about vacancy-type defect generation and evolution is rather limited. This could be ascribed to the limited traceability (larger than ~1 nm) of transmission electron microscopy routinely utilized for the study of inert gases in metals [5,6]. In this paper, we report an experimental technique with high sensitivity to the existence of vacancy-type defects, namely positron annihilation Doppler broadening spectroscopy [7]. Via analysis of the Doppler broadening spectra acquired with a slow positron beam, we characterized the defect properties in aluminum upon Xe implantation and post-annealing treatments. Our aim was to go a step further to provide information on the depth distribution, migration, and evolution of vacancy-type defects as a function of the implanted Xe dose and annealing temperatures.

2. Experiment

Prior to ion-implantation experiments, 99.999% of the Al plates were electrochemically polished in an 83% H_3PO_4 solution at 80 °C, after which 600 °C annealing was conducted under Ar ambience for 24 h in a tube furnace. Ion implantation with 380 keV Xe^+ was carried out at room temperature at four different doses: 1E15 cm^{-2}, 1E16 cm^{-2}, 5E16 cm^{-2}, and 1E17 cm^{-2}. After implantation, isochronal annealing at temperatures ranging from 100 to 600 °C was carried out, with each annealing lasting 30 min in Ar ambience.

After each step of the annealing treatment, positron-annihilation Doppler broadening measurements were carried out using a magnetically guided variable-energy positron beam (0–30 keV). The annihilation γ-rays were recorded with an intrinsic Ge detector, and Doppler broadening spectra were characterized by *S* and *W* parameters. The *S* parameter was determined as the ratio of the γ-ray counts in the range of 511.0 ± 0.7 keV to the total number of counts in the entire 511 keV peak (511.0 ± 4.2 keV). *W* parameter was defined as the ratio of the summed gamma-ray counts in the range of 513.6–517.8 keV and 504.2–508.4 keV to the total number of counts in the entire peak.

To deepen the understanding of positron annihilation characteristics in the studied specimen, the obtained positron results were fit with the VEPFIT program [8], assuming that injected positrons stop and annihilate in the sample with a three- or four-layered structure with different defect concentrations. Meanwhile, to provide supplementary information about the structural variation of the Al matrix, the Xe^+ implantation process and vacancy generation were

* Corresponding author. Tel.: +86 10 88235913; fax: +86 10 88200296.
E-mail address: yursh@ihep.ac.cn (R.S. Yu).

0169-4332/$ – see front matter © 2013 Elsevier B.V. All rights reserved.
http://dx.doi.org/10.1016/j.apsusc.2013.06.042

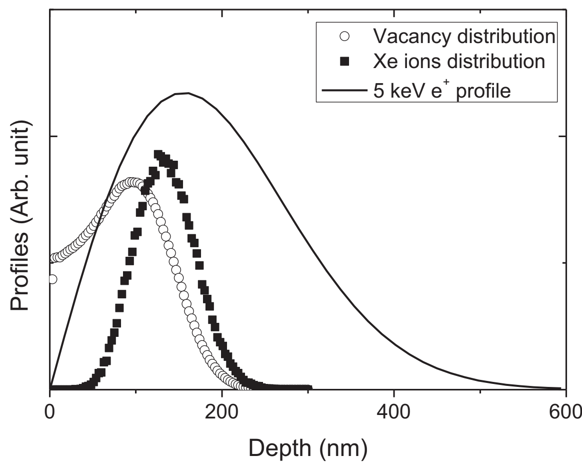

Fig. 1. Depth profile of 380 keV Xe ions and the production of vacancies obtained by SRIM calculation. The stopping probability of 5 keV incident positrons in Al is also illustrated for a visual comparison, which was calculated by $P(x) = (2x)/(x_0^2)\exp[-(x/x_0)^2]$, where $x_0 = 1.13\,x_{mean}$ and $x_{mean} = 40E^{1.6}/\rho$.

simulated with SRIM-2008 code (a program to calculate the damage and ranges of ions in matter) [9].

3. Results and discussion

Principally, in defect-free metals, an injected positron is quickly thermalized and its state can be described as a delocalized Bloch state [10]. However, due to the strong repulsion between the positive ion cores and a positron, any regions with below-average ion density, such as vacancies and other open-volume defects, will attract the positron and thus form possible trapping sites. Trapped in such a defect, the positron will experience a reduced annihilation probability from the high-momentum core electrons of surrounding atoms, in comparison with positrons in the defect-free bulk. Therefore, the positron-annihilation Doppler broadening spectra become narrower and the *S* values become larger.

As illustrated in Fig. 1, vacancies generated in Al upon 380 keV Xe^+ implantation are distributed at depths of less than 200 nm, a little less deep than the Xe ions. At the same time, one can see that positrons with 5 keV incident energy can be efficiently stopped in the entire damaged region. This firstly suggests the suitability of the positron annihilation Doppler broadening technique for characterizing vacancy-type defect properties along the ion implantation track. A second and more important point is obtained by jointly considering the experimental results shown in Fig. 2, where *S* values for all four as-implanted samples are larger than those for annealed Al, even up to 15 keV incident positron energy. This strongly suggests that vacancy distribution extends to a much deeper region than the value supplied by SRIM simulation. Such a result clearly demonstrates the high sensitivity of positrons to vacancy-type defects. And it is understandable as SRIM distribution of defects is rather roughly simulated due to many simplifications, e.g. no channeling effect considered, no diffusion and no defect interaction.

As seen in Fig. 2, along with the rise in the Xe^+ implantation dose from 1E15 to 1E17 cm^{-2}, *S* values corresponding to the damaged region are dramatically enhanced. This results from enhanced vacancy generation. Further, with the increasing implantation dose the maximum *S* in *S*(*E*) curves shifts toward to the sample surface, probably owing to the erosion of the Al target and increased scattering caused by the implanted Xe [11]. Greater damage and defect generation can reasonably be expected at the sub-surface region. Such conclusion agrees with the results obtained by VEPFIT simulation for all as-implanted samples shown in Table 1, where a reduced

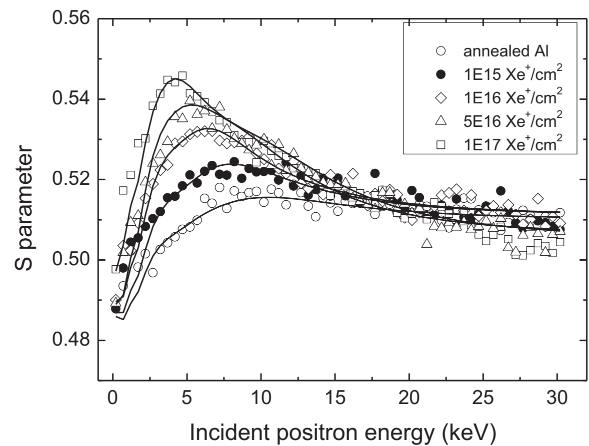

Fig. 2. Positron-annihilation Doppler broadening *S* values as a function of the incident positron energies for all as-implanted Al samples with Xe ion doses of 1E15, 1E16, 5E16, and 1E17 Xe^+cm^{-2}. Results for well-annealed Al without ion implantation are shown for comparison. The lines were obtained by VEPFIT simulation.

defect-rich layer thickness (i.e. boundary 2) and an enlarged S_{layer2} are observed under higher Xe implantation doses.

Figs. 3–5 show the post-annealing effect on Doppler broadening of the positron annihilation radiation for the three samples implanted with doses of 1E15, 1E16, and 1E17 Xe^+cm^{-2}, respectively. As in Fig. 2, the positron-annihilation Doppler broadening *S* parameter was traced as a function of the incident positron energy ranging from 0 to 30 keV. For the sample irradiated with the lowest dose, 1E15 Xe^+cm^{-2}, increasing the annealing temperature to 200 °C leads to larger *S* values. Above 300 °C, however, *S* values start to drop close to those for well-annealed Al, indicating the elimination of ion implantation induced defects. VEPFIT results shown in Table 1 also prove this, as the positron effective diffusion length ($E.D.L._2$) recovers from 140 nm to 150 nm, the value for annealed aluminum [12].

For Al implanted with a dose of 1E16 Xe^+cm^{-2}, interestingly, the increment in *S* values along with a rise in annealing temperature lasts until 500 °C. At 600 °C annealing *S* values drop close to those for as-implanted Al; nonetheless, they remain higher than for well-annealed Al. This implies that the collision cascades accompanying Xe^+ implantation produce a high density of point defects in the Al matrix, and the complete removal of irradiation damage seems impossible at such a high implantation dose.

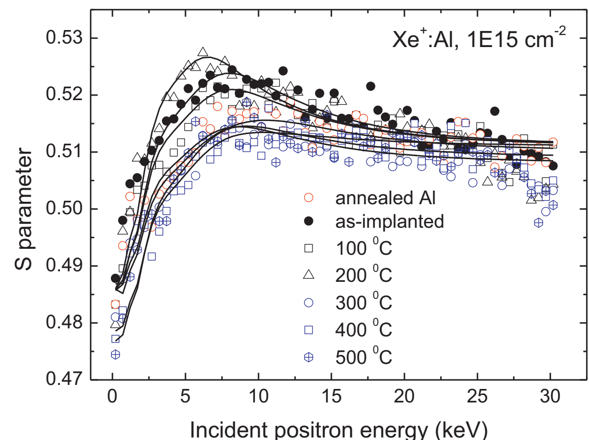

Fig. 3. Positron-annihilation Doppler broadening *S* values as a function of incident positron energies for as-implanted and post-implantation annealed Al. The Xe ion dose is 1E15 Xe^+cm^{-2} and annealing temperatures range from 100 to 500 °C. The lines were obtained by VEPFIT simulation.

Table 1
VEPFIT results for all the as-implanted as well as annealed aluminum samples subjected to xenon implantation under different doses. Effective diffusion length (E.D.L.) for positrons in the first fitting layer (5-nm thick, i.e. boundary 1 equals to 5 nm) was fixed to 20 nm.

As-implanted samples Ion dose (Xe^+cm^{-2})	Fit layers	Boundary 2 (nm)	Boundary 3 (nm)	S_{layer2}	S_{layer3}	$E.D.L._2$ (nm)	$E.D.L._3$ (nm)	$E.D.L._{Bulk}$ (nm)
1E15	3	760		0.534		140		150
1E16	3	580		0.55		130		150
5E16	4	400	980	0.568	0.526	130	140	150
1E17	4	300	1200	0.585	0.526	110	130	150
Annealed samples								
1E15	100 °C	760		0.53		140		150
	200 °C	560		0.545		142		150
	300 °C	800		0.521		142		150
	400 °C	800		0.52		150		150
	500 °C	800		0.523		150		150
1E16	100 °C	600		0.555		130		150
	200 °C	600		0.551		130		150
	300 °C	550		0.562		130		150
	400 °C	490		0.58		130		150
	500 °C	450		0.595		125		150
	600 °C	500		0.56		145		150
1E17	100 °C	118	900	0.655	0.535	100	130	150
	200 °C	200	600	0.59	0.535	110	130	150
	300 °C	200	600	0.592	0.545	110	130	150
	400 °C	200	600	0.586	0.545	110	130	150

A similar trend for S values is illustrated in Figs. 3 and 4. At an earlier stage of heat treatment, S values corresponding to the damaged region rise and their peak moves toward the sample surface. A radiation-enhanced out diffusion process of Xe atoms in metals has been observed by some researchers [11,13,14], attributed to the activation of Xe atoms by the energy dissipation of subsequently injected Xe, such that previously implanted (trapped) Xe becomes mobile. The results of the present study imply that for vacancy-type defects, a similar effect occurs during the annealing procedure. It is probable that the out diffusion of Xe and the defects are linked. Since Xe atoms are inert and extremely insoluble in Al, they tend to aggregate and be trapped by vacancies in the matrix [15,16], forming Xe_nV_m clusters (as established by work on He_nV_m clusters in Al and Si [17,18]). At higher temperatures, the migration of smaller Xe_nV_m-type defects becomes easier. This results in some coalescence to form larger ones. If this occurs in the vicinity of the surface, out diffusion and the release of previously collected Xe from vacancy traps is facilitated, since the outside vacuum acts as an unstable sink [19]. Thereby positrons tend to reside in enlarged open spaces and S values near the sample surface are enlarged. At even higher annealing temperatures, e.g. 600 °C for 1E16 Xe^+cm^{-2}, the collapse of vacancy clusters and the recrystallization of damaged regions start to play a predominant role, and S values are reduced.

For Al implanted with the highest dose, 1E17 Xe^+cm^{-2}, one can see from Fig. 5 that annealing only reduces the S parameter. The results corresponding to 100–400 °C annealing are roughly similar to each other at ~5 keV incident positron energy. Further, the largest S values characterizing defect regions for the as-implanted Al sample are equivalent to those of 500 °C annealed Al irradiated with a dose of 1E16 Xe^+cm^{-2}, i.e. representing the largest value among all samples discussed in the present study. This suggests a saturation of positron trapping in the as-implanted sample by the extensive vacancies and vacancy clusters produced by the heavy irradiation dose of 1E17 Xe^+cm^{-2}. Subsequent annealing till 400 °C could only facilitate the decomposition and partial elimination of

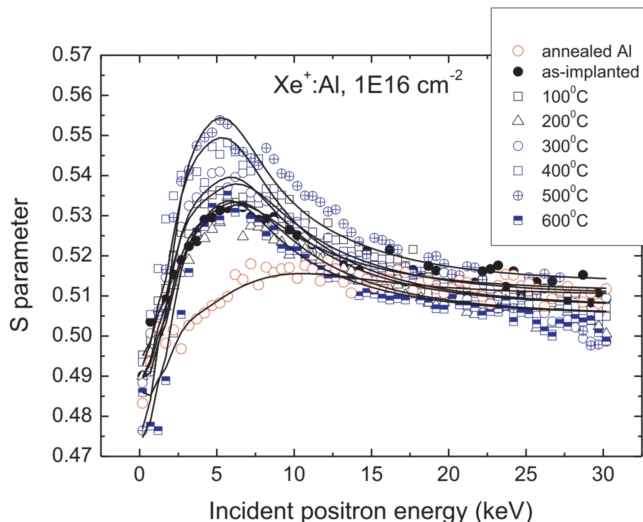

Fig. 4. Positron-annihilation Doppler broadening S values as a function of incident positron energies for as-implanted and post-implantation annealed Al. The Xe ion dose is 1E16 Xe^+cm^{-2} and annealing temperatures range from 100 to 600 °C. The lines were obtained by VEPFIT simulation.

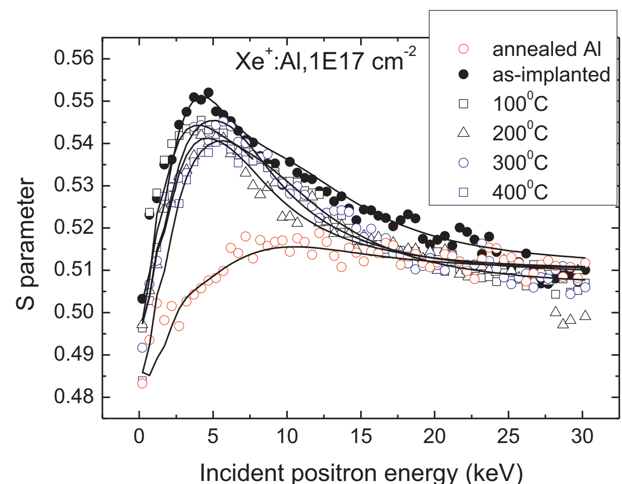

Fig. 5. Positron-annihilation Doppler broadening S values as a function of incident positron energies for as-implanted and post-implantation annealed Al. The Xe ion dose is 1E17 Xe^+cm^{-2} and annealing temperatures range from 100 to 400 °C. The lines were obtained by VEPFIT simulation.

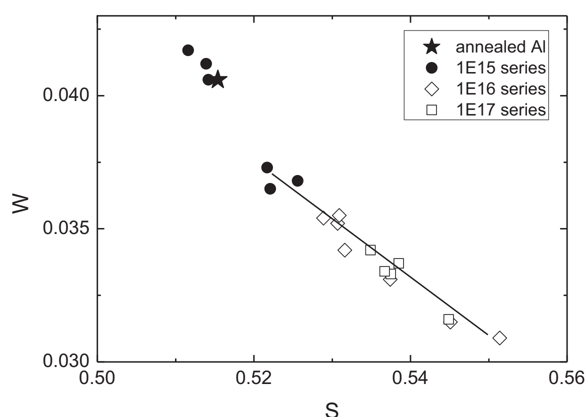

Fig. 6. *S–W* plot of characteristic points for the as-implanted as well as annealed aluminum samples implanted with ion doses of 1E15, 1E16, and 1E17 $Xe^{+}cm^{-2}$. For comparison, data for well-annealed aluminum is also illustrated. The line was drawn to guide the eyes.

large vacancy clusters and Xe_nV_m clusters, leading to the decrease in *S* values.

To further clarify the positron annihilation process, plot of characteristic *S* versus *W* for all the studied samples is examined (see Fig. 6). Evidently, except for well-annealed Al and those three specimens subjected to 1E15 $Xe^{+}cm^{-2}$ irradiation and ≥300 °C annealing (vacancies were eliminated), all the data can be roughly represented by one linear correlation, indicating the same type of positron traps, i.e. vacancy-type defects including vacancies as well as Xe_nV_m defects. A visual representation of the above postulation may be as that shown in Fig. 7, where vacancy and vacancy decorated by Xe atoms (different size of Xe_nV_m) shall be efficient trapping sites for injected positrons.

Finally, it is interesting to discuss about the possibility of positronium (Ps) formation [20,21] in Xe precipitates, i.e. Xe bubbles. Our preliminary beam-based lifetime measurements reveal that for all the as-implanted as well as subsequently annealed Al, no long lifetime component corresponding to ortho-positronium (*o*-Ps) pick-off annihilation was found (only two lifetime component analysis was suitable, and for the as-implanted 1E17 $Xe^{+}cm^{-2}$ sample, τ_{av} = 440 ps; for the 500 °C annealed Al irradiated with a dose of 1E16 $Xe^{+}cm^{-2}$, τ_{av} = 410 ps). It seems that Ps formation in the Xe bubbles embedded in Al matrix is unlikely, owing to the existence of vacancy type defects. Nonetheless, further examination of positron annihilation behavior in such material, especially using coincidence Doppler broadening (CDB) technique, seems very necessary.

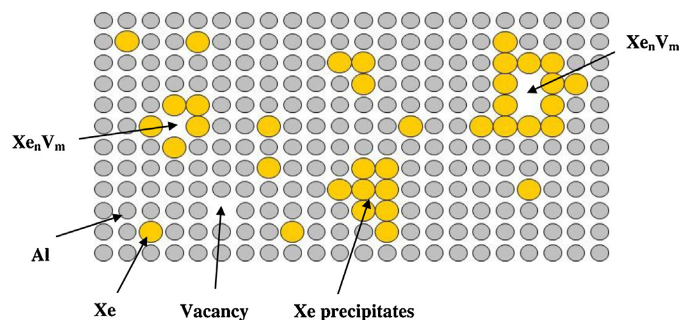

Fig. 7. Principle schematic for the microstructure of Xe ion implanted aluminum. Instead of Xe precipitates (bubbles), vacancies as well as vacancies decorated with Xe (Xe_nV_m) are the proposed trapping sites for injected positrons, which lead to the enhancement of *S* values.

4. Summary

In summary, vacancy-type defect characterization in Xe^{+}-implanted aluminum was conducted with a variable-energy positron beam. Results clearly demonstrate the high sensitivity of positrons to vacancy-type defects extending to a much deeper region than that given by SRIM simulation. With an increase in implantation dose, the defect-rich region shifts toward the sample surface. A complete recovery of structure damage for the 1E15 $Xe^{+}cm^{-2}$ irradiated sample was observed upon annealing at 300 °C. Because vacancy-defects with a lower concentration were introduced, they could be easily annealed out. Increasing the implantation dose to 1E16 and 1E17 $Xe^{+}cm^{-2}$ leads to copious defect generation, this is hardly eliminated by post-annealing due to the existence of vacancy as well as Xe_nV_m clusters. Doppler broadening of positron annihilation radiation reveals details of surface-directed migration, coalescence, and the decomposition of vacancy and Xe_nV_m clusters in the implanted samples during thermal treatments. Moreover, Ps formation inside Xe bubbles in Al matrix was not observed, as these precipitates might not be efficient positron trapping centers compared with vacancy-type defects.

Acknowledgements

R.S. Yu is grateful to the JAEA for the grant of a research fellowship. Financial support from the NSFC under grant numbers 10835006, 10705031, 11175191, and 91026006 is also acknowledged.

References

[1] A. Vom Felde, J. Fink, T. Muller-Heinzerling, J. Pfluger, B. Scheerer, G. Linker, D. Kaletta, Pressure of neon, argon, and xenon bubbles in aluminum, Physical Review Letters 53 (1984) 922–925.
[2] N. Ishikawa, M. Awaji, K. Furuya, R.C. Birtcher, C.W. Allen, HRTEM analysis of solid precipitates in Xe-implanted aluminum, Nuclear Instruments and Methods in Physics Research Section B 127/128 (1997) 123–126.
[3] D.I. Potter, C.J. Rossouw, High resolution imaging of crystalline xenon and xenon alloys in aluminum, Journal of Nuclear Materials 161 (1989) 124–131.
[4] C.W. Allen, R.C. Birtcher, S.E. Donnelly, K. Furuya, N. Ishikawa, M. Song, Migration and coalescence of Xe nanoprecipitates in Al induced by electron irradiation at 300 K, Applied Physics Letters 74 (1999) 2611–2613.
[5] J.H. Evans, D.J. Mazey, Evidence for solid krypton bubbles in copper, nickel and gold at 293 K, Journal of Physics F: Metal Physics 15 (1985) L1–L6.
[6] M. Song, K. Mitsuishi, H. Yasuda, K. Furuya, Dynamic process of nano-structured inert gas precipitates introduced with ion implantation in aluminum, Journal of Electron Microscopy 51 (2002) S211–S214.
[7] P.J. Schultz, K.G. Lynn, Interaction of positron beams with surfaces, thin films, and interfaces, Reviews of Modern Physics 60 (1988) 701–779.
[8] A. van Veen, H. Schut, M. Clement, J.M.M. de Nijsb, A. Kruseman, M.R.I. Jpma, VEPFIT applied to depth profiling problems, Applied Surface Science 85 (1995) 216.
[9] J.F. Ziegler, J.P. Biersack, M.D. Ziegler, SRIM: The Stopping and Range of Ions in Matter, SRIM Co, USA, 2008.
[10] S.E. Donnelly, J.H. Evans (Eds.), Fundamental Aspects of Inert Gases in Solids, NATO ASI Series, vol. B279, Plenum, New York, 1991.
[11] A. Mutzke, W. Eckstein, Ion fluence dependence of the Si sputtering yield by noble gas ion bombardment, Nuclear Instruments and Methods in Physics Research Section B 266 (2008) 872–876.
[12] E. Cleary, K.G. Lynn, J. Throwe, Thermal and nonthermal positron diffusion in solid and liquid aluminum, Solid State Communications 89 (1994) 747–750.
[13] K. Wittmaack, P. Blank, W. Wach, High fluence retention of noble gases implanted in silicon, Radiation Effects 39 (1978) 81–95.
[14] K. Wittmaack, H. Oppolzer, Quantitative characterization of xenon bubbles in silicon: correlation of bubble size with the damage generated during implantation, Nuclear Instruments and Methods in Physics Research Section B 269 (2011) 380–385.
[15] P.F. Barbieri, R. Landers, F.C. Marques, Electronic and structural properties of implanted xenon in amorphous silicon, Applied Physics Letters 90 (2007) 164104.
[16] M. Werner, J.A. van den Berg, D.G. Armour, G. Carter, T. Feudel, M. Herden, M. Bersani, D. Giubertoni, L. Ottaviano, C. Bongiorno, G. Mannino, P. Bailey, T.C.Q. Noakes, Shallow BF_2 implants in Xe-bombardment-preamorphized Si: the interaction between Xe and F, Applied Physics Letters 86 (2005) 151904.

[17] M. Maekawa, A. Kawasuso, Characterization of helium bubbles in Si by slow positron beam, Journal of Physics: Conference Series 225 (2010) 012032.
[18] C.A. Chen, X. Xiang, Y. Sun, C.L. Zhou, C.X. Ma, L. Wei, Vacancy-type defects near Al surface studied by slow positron annihilation spectroscopy before and after He^+ implantation, Fusion Engineering and Design 85 (2010) 734–738.
[19] N. Menzel, K. Wittmaack, Modification of stationary xenon implantation profiles in silicon by low-energy postbombardment with inert-gas ions, Nuclear Instruments and Methods in Physics Research Section B 7/8 (1985) 366–370.
[20] N. Djourelov, G. Gutierrez, H. Marinov, E. Popov, N. Toulhoat, N. Moncoffre, Y. Pipon, P. Nédélec, Xe-implanted zirconium oxycarbide studied by variable energy positron beam, Nuclear Instruments and Methods in Physics Research Section B 269 (2011) 2709–2714.
[21] N. Djourelov, B. Marchand, H. Marinov, N. Moncoffre, Y. Pipon, P. Nédélec, N. Toulhoat, D. Sillou, Variable energy positron beam study of Xe-implanted uranium oxide, Journal of Nuclear Materials 432 (2013) 287–293.